Article:
Philip, S, Martin, RV, Pierce, JR et al. (8 more authors) (2014) Spatially and seasonally resolved estimate of the ratio of organic mass to organic carbon. Atmospheric Environment, 87. 34 - 40. ISSN 1352-2310

https://doi.org/10.1016/j.atmosenv.2013.11.065

Spatially and seasonally resolved estimate of the ratio of organic matter to organic carbon

S. Philip[a,*], R. V. Martin[a, b], J. R. Pierce[c,a], J. L. Jimenez[d], Q. Zhang[e], M. R. Canagaratna[f], D. V. Spracklen[g], C. R. Nowlan[a], L. N. Lamsal[h,i], M. J. Cooper[a], N. A. Krotkov[i]

[a]Department of Physics and Atmospheric Science, Dalhousie University, Halifax, Nova Scotia, Canada

[b]Harvard-Smithsonian Center for Astrophysics, Cambridge, Massachusetts, USA

[c]Department of Atmospheric Science, Colorado State University, Fort Collins, Colorado, USA

[d]Department of Chemistry and Biochemistry, and CIRES, University of Colorado, Boulder, CO, USA

[e]Department of Environmental Toxicology, University of California, Davis, CA

[f]Aerodyne Research, Billerica, Massachusetts, USA

[g]School of Earth and Environment, University of Leeds, Leeds, UK

[h]Goddard Earth Sciences Technology and Research, Universities Space Research Association, Columbia, Maryland, USA

[i]NASA Goddard Space Flight Center, Greenbelt, Maryland, USA

* Corresponding author: S. Philip, Department of Physics and Atmospheric Science, Dalhousie University, Halifax, NS, B3H 4R2, Canada (philip.sajeev@dal.ca)

Highlights:

1. Simple method to estimate spatially and seasonally resolved OM/OC.

2. The OM/OC ratio can be estimated from satellite-derived NO_2 concentrations.

3. Parameterization developed from Aerosol Mass Spectrometer measurements.

4. OM/OC is lower in urban areas and higher in rural areas.

5. OM/OC is lower in winter and higher in summer.

Keywords: Organic aerosol, Organic carbon, NO_2, AMS, OMI, GEOS-Chem

Abstract

Particulate organic matter (OM) is of interest for air quality and climate research, but the relationship between ambient OM and organic carbon (OC) remains ambiguous both in measurements and in modeling. We present a simple method to derive an estimate of the spatially and seasonally resolved global, lower tropospheric, ratio between OM and OC. We assume ambient NO_2 concentrations as a surrogate for fresh emission which mostly determines the continental scale OM/OC ratio. For this, we first develop a parameterization for the OM/OC ratio using the primary organic aerosol (POA) fraction of total OM estimated globally from Aerosol Mass Spectrometer (AMS) measurements, and evaluate it with high mass resolution AMS data. Second, we explore the ability of ground-level NO_2 concentrations derived from the

41 OMI satellite sensor to serve as a proxy for fresh emissions that have a high POA fraction, and
42 apply NO_2 data to derive ambient POA fraction. The combination of these two methods yields an
43 estimate of OM/OC from NO_2 measurements. Although this method has inherent deficiencies
44 over biomass burning, free-tropospheric, and marine environments, elsewhere it offers more
45 information than the currently used global mean OM/OC ratios. The OMI-derived global
46 OM/OC ratio ranges from 1.3 to 2.1 (μg/μgC), with distinct spatial variation between urban and
47 rural regions. The seasonal OM/OC ratio has a summer maximum and a winter minimum over
48 regions dominated by combustion emissions. This dataset serves as a tool for interpreting organic
49 carbon measurements, and for evaluating modeling of atmospheric organics. We also develop an
50 additional parameterization for models to estimate the ratio of primary OM to OC from
51 simulated NO_x concentrations.

52

53 **1. Introduction**

54 Organic aerosols (OA) are a major constituent of fine particulate mass which affects air quality,
55 visibility, and climate. Primary OA (POA) are mostly produced by combustion sources, while
56 secondary OA (SOA) form through oxidation and partitioning of volatile organic compounds
57 from anthropogenic and biogenic sources. Ambient OA is a complex mix of thousands of
58 different organic molecules that introduces difficulties in analytical measurements, leaving large
59 measurement uncertainty (e.g., Kanakidou et al., 2005; Jimenez et al., 2009). OA contains
60 organic carbon (OC) as its major constituent and other elements such as oxygen, hydrogen and
61 nitrogen, which together with OC constitute the total organic aerosol mass. Characterization of

OA requires spatially and seasonally resolved information about the ratio of OA with OC (OA/OC, also commonly written as OM/OC, where OM is "organic mass", a synonym of OA).

Traditional ground-based impaction or filter-based instruments routinely measure OC using different analytic methods (e.g., Hand et al., 2012), but not OM due to difficulties in characterizing different components of OM. Other specific techniques that measure OM directly, such as Fourier Transform Infrared spectroscopy (FTIR) (Russell et al., 2009) and solvent extraction techniques (El-Zanan et al., 2005), are not used extensively. A wide range of literature is available on the methods to determine the OM/OC ratio, and it is a broadly debated issue. A common practice to interpret OC measurements is through the use of a continental mean value for the OM/OC ratio (such as 1.4 (Grosjean and Friedlander 1975; White and Roberts, 1977), 1.6 (Malm et al., 1994), 1.4-2.1 (Turpin and Lim, 2001), and 1.8 (Hand et al., 2012) for North America). The spatial and seasonal variation in the OM/OC ratio is often neglected in the interpretation of measurement data due to insufficient information (e.g., Hand et al., 2012).

These global-mean values are frequently used in aerosol models to convert between POA and OM (e.g., Park et al., 2003). This is because most global and regional models simulate POA as OC. Despite notable developments for simulating the oxidative aging of OM (Simon et al., 2012), most models do not yet readily predict the OM/OC ratio. A spatially and seasonally varying estimate of the OM/OC ratio should help interpret simulated organic aerosols.

The OM/OC ratio is directly related to the O/C ratio in the organic mass, since the contribution of non-oxygen elements to the OM/OC ratio is generally small, and both ratios increase with chemical aging of OA (Aiken et al., 2008; Pang et al., 2006). OM/OC has seasonal and spatial variation depending on the sources of POA and SOA and their degree of aging. The Aerosol

Mass Spectrometer (AMS) offers quantitative determination of the size-resolved submicron OM at high temporal resolution through mass spectrometry (Jimenez et al., 2003; Canagaratna et al., 2007). Factor analysis of the AMS spectra can differentiate POA such as hydrocarbon-like OA (HOA) and several types of oxygenated OA (OOA) (Zhang et al., 2005a) that are typically SOA surrogates (Zhang et al., 2007, 2011). POA has lower OM/OC than SOA, and fresh SOA has lower OM/OC than aged SOA (Aiken et al., 2008).

The oxidative aging of organics may be indirectly estimated through different proxies. Both NO_x and submicron POA are mainly emitted from combustion processes. NO_x is oxidized in the atmosphere with a timescale of about a day. Over regional scales OA is dominated by SOA, and anthropogenic SOA is also formed with a timescale of about a day and in amounts much larger than the originally emitted POA (DeCarlo et al., 2010). Globally most SOA may be due to anthropogenic enhancement of biogenic SOA, which is also thought to have a similar timescale of formation (Goldstein et al., 2009; Spracklen et al., 2011). Once formed, all types of SOA appear to age with a characteristic timescale of about 1-2 days, increasing the OM/OC ratio (Jimenez et al., 2009). Given the similar spatial emission patterns and timescales, we explore ambient NO_2 concentrations as a surrogate for the POA/OA fraction and thus OM/OC ratios.

Here, we introduce a parameterization for OM/OC based on the POA fraction estimated from AMS measurements (section 2.1), test global ground-level NO_2 and NO_x concentrations as a proxy for POA and thus OM/OC (sections 2.2 and 2.3), and develop a gridded dataset of the seasonally varying OM/OC ratio (section 2.4). We describe the spatially and seasonally varying satellite-derived OM/OC in section 3.

2. Materials and methods

2.1. Primary OA fraction of the AMS data to predict OM/OC

We first explore a method to derive OM/OC. For this, we use the POA fraction of the AMS data as a proxy for combustion emissions (where combustion emissions can then be determined from the measurements of co-emitted species such as NO_x). Aiken et al. (2008) demonstrate a method to use high-resolution time-of-flight AMS ambient OA measurements to directly quantify the OM/OC ratio. Aiken et al. (2008) report a high correlation for OM/OC versus O/C (r = 0.998), quantify the OM/OC ratio for urban POA as ~1.3, and find that for OOA the OM/OC ratio varies from 1.9 to 2.4. Per the timescale discussion above, f_{POA} (the ratio of POA, determined from factor analysis of AMS spectra (Zhang et al., 2011), to the total measured OA) is expected to be inversely related to OM/OC. Therefore, we parameterize OM/OC from AMS using f_{POA},

$$OM/OC = 1.3 \times f_{POA} + 2.1 \times (1 - f_{POA}) \quad (1)$$

This method assumes that POA has an OM/OC ratio of 1.3 and OOA has a value of 2.1. However it should be noted that the OM/OC values for OOA can range from 1.9 to 2.4, and therefore our assumption introduces an uncertainty to the OM/OC estimates from the equation 1. An independent evaluation with direct OM/OC estimates from the AMS quantifies this uncertainty (± 0.2 μg/μgC) as described below. We collected nine published high mass resolution campaign-mean AMS-estimated f_{POA} and AMS-measured OM/OC data from field campaigns to evaluate this parameterization. Figure 1 shows the scatter plot of AMS OM/OC and f_{POA}. It includes a representation of a typical urban POA with OM/OC ratio of 1.3 (f_{POA} = 1). We plotted equation 1 over this scatter plot (black line). The scatter points (OM/OC) are

approximately within ± 0.2 (μg/μgC) from the solid black line. This confirms the validity of the predicted relation in equation 1. Moreover, the high correlation (r = - 0.91) supports the linear relation between AMS f_{POA} and OM/OC in the continental boundary layer across a variety of regions. However, we caution that there are few free-tropospheric, biomass burning or marine boundary layer observations in this dataset. OM/OC values can exceed 2.1 outside of the continental boundary layer (Sun et al., 2009) and from biomass burning (Turpin and Lim, 2001). Thus, this parameterization may underestimate OM/OC in those regions. Although the relation in equation 1 offers another estimate (indirect) of OM/OC over AMS locations, this relation is developed only to generate OM/OC from NO_x measurements (section 3). More reliable methods to estimate OM/OC from AMS are already available (for example, publications listed in the Figure 1 caption).

Spracklen et al. (2011) and Zhang et al. (2007) collected AMS POA and OOA data for 47 approximately month-long observation campaigns over 37 locations. However, this dataset does not have reliable high mass resolution OM/OC measurements to evaluate equation 1. Nevertheless, this dataset has reliable POA fraction data for a broad range of locations. The prediction model in equation 1 can be applied to f_{POA} estimates of these 47 campaign mean dataset to generate an indirect OM/OC dataset. Figure 2 shows these global AMS measurements of OA (top left), POA (top right), f_{POA} (bottom left), and the derived OM/OC ratio (bottom right). f_{POA} is high over regions with fresh anthropogenic emissions. The OM/OC ratio typically ranges from 1.7 to 2.1.

We also considered the OM/OC ratio as estimated through a multiple regression analysis of IMPROVE data (Simon et al., 2011). However, the OM/OC ratio estimated from AMS and

IMPROVE measurements differs from each other (r = 0.4, RMSE = 0.13 μg/μgC, number of points = 13), and the difference is not well understood. The O/C from the AMS is a more direct measurement, whereas the OM from IMPROVE is based on the measured OC plus extra mass needed to get closure between the total characterized mass and the total measured mass (Aiken et al., 2008; Simon et al., 2011). The inaccuracy of OC and inorganic mass measurements by IMPROVE filter techniques, and the subtraction of two large numbers introduce errors in the OM/OC calculation (Simon et al., 2011). In addition, filter measurements tend to suffer loss of semivolatile species (especially during warm seasons) and condensation of volatile organic compounds. Real time AMS measurements are less influenced by gas-particle partitioning of semivolatile species. Thus we focus exclusively on AMS data for the remainder of this manuscript.

2.2. Nitrogen oxides as a proxy for primary OA fraction

Primary organic aerosol has major sources from local combustion processes. Several studies reported the high correlation of AMS-estimated POA with nitrogen oxide species (e.g., Zhang et al. 2005b; Sun et al., 2011; Ge et al., 2012). Therefore, the fractionation of ambient OA to primary and oxygenated components can be determined indirectly from the measurements of NO_x. Given the correlation between POA and NO_x, here we explore the relationship between AMS POA fraction measurements, and a spatially coincident modeled NO_x climatology to develop a proxy for the POA fraction and then the OM/OC ratio. We use the GEOS-Chem (http://geos-chem.org) global three-dimensional chemical transport model to test the correlations between AMS-estimated f_{POA} and co-emitted combustion related species. GEOS-Chem includes a detailed simulation of oxidant-aerosol chemistry as described in the Appendix.

We tested the spatial correlation between AMS-estimated f_{POA} and coincident GEOS-Chem simulations of NO_x (r = 0.73), NO_2 (r = 0.74), hydrophobic OC (r = 0.42), BC (r = 0.57), and CO (r = 0.15). The significant correlation for NO_x supports the use of this species as a proxy for the AMS POA fraction. Therefore, we assume that the typical continental POA fraction is a function of NO_x concentrations.

2.3. Ambient primary OA fraction estimate from satellite-derived nitrogen dioxide concentration

Given the significant correlation between modeled nitrogen oxides and observed POA fraction, we further compare AMS f_{POA} with satellite retrievals of NO_2 which offer finer spatial information than the model. Advancements in satellite remote sensing over the last decade yield accurate retrievals of global NO_2 column concentrations at moderate spatial resolution (Boersma et al., 2011; Bucsela et al., 2013). The NO_2 column concentrations are closely related to local NO_x emission (Martin et al., 2003a) and ground-level NO_2 concentrations (Lamsal et al., 2008). We relate these NO_2 concentrations with the POA fraction at ground-level. We begin with NO_2 columns retrieved by Bucsela et al. (2013) for years 2005-2008 from the Dutch-Finnish built Ozone Monitoring Instrument (OMI) sensor aboard the NASA Aura satellite. We retain column data that have cloud fraction < 0.3, solar zenith angle < 78^0 and near-nadir viewing angle (scan positions 7 to 53 out of 60).

We use the daily coincident ratio of column density to ground-level concentration simulated with the GEOS-Chem model to derive daily ground-level NO_2 concentrations at a spatial resolution of 0.1^0 x 0.1^0 following Lamsal et al. (2008, 2010). Ground-level NO_2 concentrations derived from

this approach exhibit significant temporal (r = 0.30 - 0.96, mean r = 0.69) and spatial (r = 0.78) correlation versus in situ measurements at 307 sites across North America (Lamsal et al., 2013).

We sampled the long-term monthly mean OMI-derived ground-level NO_2 mixing ratio (at a spatial resolution of 0.1^0 x 0.1^0) with the spatially coincident AMS-estimated POA fraction. Figure 3 shows the scatter plot of OMI NO_2 versus AMS f_{POA}. Similar to model comparisons mentioned above, the correlation for these two species is significant (r = 0.73). Excluding outliers (New York City, summer 2001; New York City, winter 2004; and Vancouver, Canada, August 2001 campaigns) increases it further up (r = 0.87). This supports the utility of OMI nitrogen dioxide measurements to predict the fractionation of ambient OA.

A linear relation can be used to derive ambient f_{POA} from OMI NO_2 data given their high correlation. We used the correlation statistics obtained for a reduced major axis regression between the AMS f_{POA} and OMI NO_2 (r = 0.73, slope = 11.32, offset = -0.77, N = 47) to fit a line. We then compared f_{POA} estimated from OMI NO_2 (using the linear fit) against 47 AMS f_{POA} data, and obtained an RMSE of 0.31 (r = 0.73, slope = 1.0, offset = 0, N = 47). However, we note that a fast increase of f_{POA} at low NO_2 concentrations is more consistent with Figure 3. OMI NO_2 is almost constant for f_{POA} between 0 and 0.2, and increasing thereafter. Therefore we test a non linear relation here.

The ground-level f_{POA} and the OMI NO_2 data (ppb) follow,

$$f_{POA} = ((\text{OMI } NO_2 - 0.2) / 15)^{0.5} \quad (2)$$

We reproduced the f_{POA} values from OMI NO_2 data using equation 2, and compared with 47 AMS f_{POA}, and obtained a high correlation (r = 0.85, slope = 1.11, offset = -0.02, RMSE = 0.25,

N = 47). The RMSE of 0.31 for a linear fit exceeds the RMSE of 0.25 for the non-linear fit. Therefore, equation 2 is a good approximation of the relation between the fractionation of ambient OA versus NO_2 concentrations over a broad region.

2.4. Global OM/OC from satellite-derived and modeled nitrogen oxides

Having predicted (equations 1 and 2) and evaluated the relation for AMS OM/OC versus AMS f_{POA} (section 2.1), and AMS f_{POA} versus OMI NO_2 (section 2.3), it is straightforward to derive seasonally varying maps of the global OM/OC ratio. Equation 1 and 2 leads to an empirical OM/OC prediction model as,

$$OM/OC = 2.1 - 0.8 \times ((OMI\ NO_2 - 0.2) / 15)^{0.5} \quad (3)$$

We use monthly mean OMI-derived ground-level NO_2 concentrations (ppb) for 2005-2008 to produce a global climatology of the OM/OC ratio using equation (3). For $NO_2 < 0.2$, the OM/OC ratio is 2.1 which is consistent with a ratio over regions which lack primary emission. We imposed a lower limit of 1.3 to avoid unrealistic (f_{POA} exceeding 1) values for extremely high NO_2 conditions. A cross validation of the OMI-derived long-term monthly mean OM/OC product with the 47 AMS- derived OM/OC (from AMS f_{POA} using equation 1) data shows an RMSE of 0.06 μg/μgC (r = 0.85, slope = 1.11, offset = -0.21, N = 47).

Similarly, we create a prediction model from the GEOS-Chem NO_x concentrations,

$$OM/OC = 2.1 - 0.8 \times ((NO_x - 0.5) / 18)^{0.6} \quad (4)$$

231 The GEOS-Chem NO_x estimated OM/OC also has significant agreement (r = 0.74, slope = 1.08,
232 offset = -0.15, RMSE = 0.08 μg/μgC) with the AMS data. Hence, model simulations of NO_x also
233 can be used as a proxy for OM/OC.

234 **3. Discussion of the global OM/OC ratio**

235 Figure 4 shows seasonal maps of the predicted OM/OC ratio based on the OMI-derived NO2
236 concentration climatology. Maximum OM/OC ratios above 1.9 are found in regions with low
237 NOx emissions. Urban and industrial regions of the Northern Hemisphere tend to have lower
238 OM/OC ratios. Fresh urban OA emission from transportation leads to low values for OM/OC in
239 Eastern North America. The southeast U.S. with biogenic SOA production has high OM/OC
240 values. Biomass burning regions have high predicted OM/OC ratios which are coincidently
241 consistent with expectations; future work should extend this parameterization to explicitly
242 represent the enhanced OM/OC from fires. Biases due to soil NO_x emissions are not apparent,
243 due to the diffuse nature of the source. Annual mean values for urban (~1.5 μg/μgC) and rural
244 (~2.0 μg/μgC) regions are broadly consistent with the values recommended by Turpin and Lim
245 (2001). FTIR spectroscopy methods yield annual mean values of 1.9-2.0 μg/μgC over both
246 Pittsburg (Polidori et al. 2008) and a rural site in Hungary (Kiss et al. 2002), which close to our
247 regional estimate of 1.8 μg/μgC.

248 The OM/OC ratio has a winter minimum and summer maximum over polluted regions. The high
249 summer OM/OC in this dataset reflects lower NO_x and f_{POA} in summer compared to winter. In
250 general, high temperatures and sunlight in summer lead to high oxidant availability and enhanced
251 photochemistry. The resulting oxidative aging of POA and enhanced SOA formation increase the

summertime OM/OC ratio compared to winter. The lower winter OM/OC is due to lower oxygen content in the aged OA. Simon et al., (2011) also find similar seasonality for the OM/OC ratio despite differences in magnitude. Xing et al. (2013) used chemical analysis of organic compounds extracted from $PM_{2.5}$ to find OM/OC ratios for 14 Chinese cities in summer of 1.75 ± 0.13 μg/μgC compared with our estimate of ~1.8 μg/μgC, and in winter of 1.59 ± 0.18 μg/μgC compared with our estimate of ~1.6 μg/μgC. Hence, we conclude that the global annual mean values for urban and rural regions, and its seasonal variation over urban regions are broadly consistent with the values recommended by several other studies.

4. Conclusions

We developed a simple technique to estimate the spatial and seasonal variation of the global OM/OC ratio. OMI NO_2 observations were used to represent air mass age and scaled to AMS observations. The resultant dataset appears to generally represent the OM to OC ratio in most of the continental boundary layer. Underestimates are expected in biomass burning, marine and free tropospheric environments. Nonetheless the dataset should serve as an improvement over the commonly used global values for OM/OC. This work would benefit from more AMS measurements of the OM/OC ratio across multiple seasons and regions. Ongoing efforts to explicitly simulate oxidative aging of OA should ultimately yield a more complete representation of OM/OC.

Appendix

The GEOS-Chem (version 9-01-03; http://geos-chem.org) is a global three-dimensional chemical transport model driven with assimilated meteorological data from the Goddard Earth Observing

System (GEOS-5) at the NASA Global Modeling Assimilation Office (GMAO). We conduct our simulations at a spatial resolution of 2^0 x 2.5^0 for the years 2005-2008. The lowest layer of the model is approximately 130 meters with a total of 47 levels from the Earth's surface to the top of the atmosphere. We use full mixing of species below the mixed layer depth, with a correction to the GEOS-5 predicted mixed layer depth (Heald et al., 2012; Walker et al., 2012). We use a timestep of 15 minutes for dynamical processes (transport and convection), and a timestep of 60 minutes for chemical processes and emissions.

GEOS-Chem contains a detailed simulation of HO_x-NO_x-VOC-ozone-aerosol chemistry (Bey et al., 2001; Park et al., 2004). Mao et al. (2010) describe the GEOS-Chem chemical mechanism in detail. The simulation of secondary inorganic ions is directly coupled with gas phase chemistry (Park et al., 2004). Aerosol-gas interactions are simulated through heterogeneous chemistry (Jacob, 2000) with updated aerosol uptake of N_2O_5 (Evans and Jacob, 2005) and HO_2 (Thornton et al., 2008), aerosol extinction effects on photolysis rates (Martin et al., 2003b), the partitioning of aerosols from gas using the ISORROPIA II thermodynamic scheme (Fontoukis and Nenes, 2007) as implemented by Pye et al. (2009), and gas-aerosol partitioning of semivolatile products of VOC oxidation (Henze et al., 2006, 2008; Liao et al., 2007).

Anthropogenic NO_x emission inventories are from the EDGAR v32-FT2000 global inventory for 2000 (Olivier et al., 2005), with regional overwrites over the U.S. (Environmental protection Agency-National Emissions Inventory 2005), Canada (CAC; http://www.ec.gc.ca/pdb/cac/), Mexico (BRAVO; Kuhns et al., 2005), Europe (EMEP; http://www.emep.int/), and East Asia (Zhang et al., 2009). Emissions are scaled to subsequent years on the basis of energy statistics (van Donkelaar et al., 2008) and after 2006 with OMI NO_2 data (Lamsal et al., 2011). Other

major non-anthropogenic land NO_x emissions include biomass burning emissions (GFED-3; Mu et al., 2011) and soil emissions (Yienger and Levy, 1995; Wang et al., 1998).

Acknowledgements

This work was supported by NSERC. JLJ was supported by DOE (BER/ASR) DE SC0006035/DE-SC0006711/DE-FG02-11ER65293. QZ was supported by DE-FG02-11ER65293. We thank Aaron van Donkelaar and Ian Folkins for useful comments.

References

Aiken, A.C., Decarlo, P.F., Kroll, J.H., Worsnop, D.R., Huffman, J.A., Docherty, K.S., Ulbrich, I.M., Mohr, C., Kimmel, J.R., Sueper, D., Sun, Y., Zhang, Q., Trimborn, A., Northway, M., Ziemann, P.J., Canagaratna, M.R., Onasch, T.B., Alfarra, M.R., Prevot, A.S.H., Dommen, J., Duplissy, J., Metzger, A., Baltensperger, U., Jimenez, J.L., 2008. O/C and OM/OC ratios of primary, secondary, and ambient organic aerosols with high-resolution time-of-flight aerosol mass spectrometry. Environmental science & technology 42, 4478-4485.

Bey, I., Jacob, D.J., Yantosca, R.M., Logan, J.A., Field, B.D., Fiore, A.M., Li, Q.B., Liu, H.G.Y., Mickley, L.J., Schultz, M.G., 2001. Global modeling of tropospheric chemistry with assimilated meteorology: Model description and evaluation. Journal of Geophysical Research-Atmospheres 106,

Boersma, K.F., Eskes, H.J., Dirksen, R.J., van der A, R.J., Veefkind, J.P., Stammes, P., Huijnen, V., Kleipool, Q.L., Sneep, M., Claas, J., Leitao, J., Richter, A., Zhou, Y., Brunner, D., 2011. An improved tropospheric NO2 column retrieval algorithm for the ozone monitoring instrument. Atmospheric Measurement Techniques 4, 1905-1928.

Bucsela, E. J., Krotkov, N. A., Celarier, E. A., Lamsal, L. N., Swartz, W. H., Bhartia, P. K., Boersma, K. F., Veefkind, J. P., Gleason, J. F., and Pickering, K. E., 2013. A new stratospheric and tropospheric NO2 retrieval algorithm for nadir-viewing satellite instruments: applications to OMI. Atmos. Meas. Tech. Discuss., 6, 1361-1407, doi:10.5194/amtd-6-1361-2013.

Canagaratna, M.R., Jayne, J.T., Jimenez, J.L., Allan, J.D., Alfarra, M.R., Zhang, Q., Onasch, T.B., Drewnick, F., Coe, H., Middlebrook, A., Delia, A., Williams, L.R., Trimborn, A.M., Northway, M.J., DeCarlo, P.F., Kolb, C.E., Davidovits, P., Worsnop, D.R., 2007. Chemical and microphysical characterization of ambient aerosols with the aerodyne aerosol mass spectrometer. Mass spectrometry reviews 26, 185-222.

DeCarlo, P.F., Ulbrich, I.M., Crounse, J., de Foy, B., Dunlea, E.J., Aiken, A.C., Knapp, D., Weinheimer, A.J., Campos, T., Wennberg, P.O., Jimenez, J.L., 2010. Investigation of the sources and processing of organic aerosol over the central mexican plateau from aircraft measurements during MILAGRO. Atmospheric Chemistry and Physics 10, 5257-5280.

Docherty, K.S., Aiken, A.C., Huffman, J.A., Ulbrich, I.M., DeCarlo, P.F., Sueper, D., Worsnop, D.R., Snyder, D.C., Peltier, R.E., Weber, R.J., Grover, B.D., Eatough, D.J., Williams, B.J., Goldstein, A.H., Ziemann, P.J., Jimenez, J.L., 2011. The 2005 study of organic aerosols at riverside (SOAR-1): Instrumental intercomparisons and fine particle composition. Atmospheric Chemistry and Physics 11, 12387-12420.

El-Zanan, H.S., Lowenthal, D.H., Zielinska, B., Chow, J.C., Kumar, N., 2005. Determination of the organic aerosol mass to organic carbon ratio in IMPROVE samples. Chemosphere 60, 485-496.

Evans, M.J. and Jacob, D.J., 2005. Impact of new laboratory studies of N(2)O(5) hydrolysis on global model budgets of tropospheric nitrogen oxides, ozone, and OH. Geophysical Research Letters 32, L09813.

Fountoukis, C. and Nenes, A., 2007. ISORROPIA II: A computationally efficient thermodynamic equilibrium model for K+-Ca2+-Mg2+-nh(4)(+)-na+-SO42--NO3--cl--H2O aerosols. Atmospheric Chemistry and Physics 7, 4639-4659.

Ge, X., Setyan, A., Sun, Y., Zhang, Q., 2012. Primary and secondary organic aerosols in fresno, california during wintertime: Results from high resolution aerosol mass spectrometry. Journal of Geophysical Research-Atmospheres 117, D19301.

Goldstein, A.H., Koven, C.D., Heald, C.L., Fung, I.Y., 2009. Biogenic carbon and anthropogenic pollutants combine to form a cooling haze over the southeastern united states. Proceedings of the National Academy of Sciences of the United States of America 106, 8835-8840.

Grosjean, D. and Friedlander, S.K., 1975. Gas-particle distribution factors for organic and other pollutants in los-angeles atmosphere. Journal of the Air Pollution Control Association 25, 1038-1044.

Hand, J.L., Schichtel, B.A., Pitchford, M., Malm, W.C., Frank, N.H., 2012. Seasonal composition of remote and urban fine particulate matter in the united states. Journal of Geophysical Research-Atmospheres 117, D05209.

Hayes, P.L. et al., 2013. Aerosol Composition and Sources in Los Angeles During the 2010 CalNex Campaign. Journal of Geophysical Research-Atmospheres, doi:10.1002/jgrd.50530.

Heald, C.L., Collett, J.L.,Jr., Lee, T., Benedict, K.B., Schwandner, F.M., Li, Y., Clarisse, L., Hurtmans, D.R., Van Damme, M., Clerbaux, C., Coheur, P.-., Philip, S., Martin, R.V., Pye, H.O.T., 2012. Atmospheric ammonia and particulate inorganic nitrogen over the united states. Atmospheric Chemistry and Physics 12, 10295-10312.

Henze, D.K., Seinfeld, J.H., Ng, N.L., Kroll, J.H., Fu, T.-., Jacob, D.J., Heald, C.L., 2008. Global modeling of secondary organic aerosol formation from aromatic hydrocarbons: High- vs. low-yield pathways. Atmospheric Chemistry and Physics 8, 2405-2420.

Henze, D.K. and Seinfeld, J.H., 2006. Global secondary organic aerosol from isoprene oxidation. Geophysical Research Letters 33, L09812.

Huang, X.-., He, L.-., Hu, M., Canagaratna, M.R., Kroll, J.H., Ng, N.L., Zhang, Y.-., Lin, Y., Xue, L., Sun, T.-., Liu, X.-., Shao, M., Jayne, J.T., Worsnop, D.R., 2011. Characterization of submicron aerosols at a rural site in pearl river delta of china using an aerodyne high-resolution aerosol mass spectrometer. Atmospheric Chemistry and Physics 11, 1865-1877.

Huang, X.-., He, L.-., Hu, M., Canagaratna, M.R., Sun, Y., Zhang, Q., Zhu, T., Xue, L., Zeng, L.-., Liu, X.-., Zhang, Y.-., Jayne, J.T., Ng, N.L., Worsnop, D.R., 2010. Highly time-resolved chemical characterization of atmospheric submicron particles during 2008 beijing olympic games using an aerodyne high-resolution aerosol mass spectrometer. Atmospheric Chemistry and Physics 10, 8933-8945.

Jacob, D.J., 2000. Heterogeneous chemistry and tropospheric ozone. Atmospheric Environment 34, 2131-2159.

Jimenez, J.L., Canagaratna, M.R., Donahue, N.M., Prevot, A.S.H., Zhang, Q., Kroll, J.H., DeCarlo, P.F., Allan, J.D., Coe, H., Ng, N.L., Aiken, A.C., Docherty, K.S., Ulbrich, I.M., Grieshop, A.P., Robinson, A.L., Duplissy, J., Smith, J.D., Wilson, K.R., Lanz, V.A., Hueglin, C., Sun, Y.L., Tian, J., Laaksonen, A., Raatikainen, T., Rautiainen, J., Vaattovaara, P., Ehn, M., Kulmala, M., Tomlinson, J.M., Collins, D.R., Cubison, M.J., Dunlea, E.J., Huffman, J.A., Onasch, T.B., Alfarra, M.R., Williams, P.I., Bower, K., Kondo, Y., Schneider, J., Drewnick, F., Borrmann, S., Weimer, S., Demerjian, K., Salcedo, D., Cottrell, L., Griffin, R., Takami, A., Miyoshi, T., Hatakeyama, S., Shimono, A., Sun, J.Y., Zhang, Y.M., Dzepina, K., Kimmel, J.R., Sueper, D., Jayne, J.T., Herndon, S.C., Trimborn, A.M., Williams, L.R., Wood, E.C., Middlebrook, A.M., Kolb, C.E., Baltensperger, U., Worsnop, D.R., 2009. Evolution of organic aerosols in the atmosphere. Science 326, 1525-1529.

Jimenez, J.L., Jayne, J.T., Shi, Q., Kolb, C.E., Worsnop, D.R., Yourshaw, I., Seinfeld, J.H., Flagan, R.C., Zhang, X.F., Smith, K.A., Morris, J.W., Davidovits, P., 2003. Ambient aerosol sampling using the aerodyne aerosol mass spectrometer. Journal of Geophysical Research-Atmospheres 108, 8425.

Kanakidou, M., Seinfeld, J.H., Pandis, S.N., Barnes, I., Dentener, F.J., Facchini, M.C., Van Dingenen, R., Ervens, B., Nenes, A., Nielsen, C.J., Swietlicki, E., Putaud, J.P., Balkanski, Y., Fuzzi, S., Horth, J., Moortgat, G.K., Winterhalter, R., Myhre, C.E.L., Tsigaridis, K., Vignati, E., Stephanou, E.G., Wilson, J., 2005. Organic aerosol and global climate modelling: A review. Atmospheric Chemistry and Physics 5, 1053-1123.

Kiss, G., Varga, B., Galambos, I., Ganszky, I., 2002. Characterization of water-soluble organic matter isolated from atmospheric fine aerosol. Journal of Geophysical Research-Atmospheres 1107(D21), 8339.

Kuhns, H., Knipping, E.M., Vukovich, J.M., 2005. Development of a united states-mexico emissions inventory for the big bend regional aerosol and visibility observational (BRAVO) study. Journal of the Air & Waste Management Association 55, 677-692.

Lamsal, L.N., Martin, R.V., Parrish, D.D., Krotkov, N.A., 2013. Scaling relationship for NO2 pollution and urban population size: A satellite perspective. Environmental science & technology 47, 7855-61.

Lamsal, L.N., Martin, R.V., Padmanabhan, A., van Donkelaar, A., Zhang, Q., Sioris, C.E., Chance, K., Kurosu, T.P., Newchurch, M.J., 2011. Application of satellite observations for timely updates to global anthropogenic NOx emission inventories. Geophysical Research Letters 38, L05810.

Lamsal, L.N., Martin, R.V., van Donkelaar, A., Celarier, E.A., Bucsela, E.J., Boersma, K.F., Dirksen, R., Luo, C., Wang, Y., 2010. Indirect validation of tropospheric nitrogen dioxide retrieved from the OMI satellite instrument: Insight into the seasonal variation of nitrogen oxides at northern midlatitudes. Journal of Geophysical Research-Atmospheres 115, D05302.

Lamsal, L.N., Martin, R.V., van Donkelaar, A., Steinbacher, M., Celarier, E.A., Bucsela, E., Dunlea, E.J., Pinto, J.P., 2008. Ground-level nitrogen dioxide concentrations inferred from the satellite-borne ozone monitoring instrument. Journal of Geophysical Research-Atmospheres 113, D16308.

Liao, H., Henze, D.K., Seinfeld, J.H., Wu, S., Mickley, L.J., 2007. Biogenic secondary organic aerosol over the united states: Comparison of climatological simulations with observations. Journal of Geophysical Research-Atmospheres 112, D06201.

Malm, W.C., Sisler, J.F., Huffman, D., Eldred, R.A., Cahill, T.A., 1994. Spatial and seasonal trends in particle concentration and optical extinction in the united-states. Journal of Geophysical Research-Atmospheres 99, 1347-1370.

Mao, J., Jacob, D.J., Evans, M.J., Olson, J.R., Ren, X., Brune, W.H., St Clair, J.M., Crounse, J.D., Spencer, K.M., Beaver, M.R., Wennberg, P.O., Cubison, M.J., Jimenez, J.L., Fried, A., Weibring, P., Walega, J.G., Hall, S.R., Weinheimer, A.J., Cohen, R.C., Chen, G., Crawford, J.H., McNaughton, C., Clarke, A.D., Jaegle, L., Fisher, J.A., Yantosca, R.M., Le Sager, P., Carouge, C., 2010. Chemistry of hydrogen oxide radicals (HOx) in the arctic troposphere in spring. Atmospheric Chemistry and Physics 10, 5823-5838.

Martin, R.V., Jacob, D.J., Chance, K., Kurosu, T.P., Palmer, P.I., Evans, M.J., 2003a. Global inventory of nitrogen oxide emissions constrained by space-based observations of NO2 columns. Journal of Geophysical Research-Atmospheres 108, 4537.

Martin, R.V., Jacob, D.J., Yantosca, R.M., Chin, M., Ginoux, P., 2003b. Global and regional decreases in tropospheric oxidants from photochemical effects of aerosols. Journal of Geophysical Research-Atmospheres 108, 4097.

Mu, M., Randerson, J.T., van der Werf, G.R., Giglio, L., Kasibhatla, P., Morton, D., Collatz, G.J., DeFries, R.S., Hyer, E.J., Prins, E.M., Griffith, D.W.T., Wunch, D., Toon, G.C., Sherlock, V., Wennberg, P.O., 2011. Daily and 3-hourly variability in global fire emissions and consequences for atmospheric model predictions of carbon monoxide. Journal of Geophysical Research-Atmospheres 116, D24303.

Olivier, J.G.J. et al., 2005. Recent trends in global greenhouse gas emissions: regional trends 1970-2000 and spatial distribution of key sources in 2000. Env. Sc., 2 (2-3), 81-99. DOI: 10.1080/15693430500400345.

Pang, Y., Turpin, B.J., Gundel, L.A., 2006. On the importance of organic oxygen for understanding organic aerosol particles. Aerosol Science and Technology 40, 128-133.

Park, R.J., Jacob, D.J., Field, B.D., Yantosca, R.M., Chin, M., 2004. Natural and transboundary pollution influences on sulfate-nitrate-ammonium aerosols in the united states: Implications for policy. Journal of Geophysical Research-Atmospheres 109, D15204.

Park, R.J., Jacob, D.J., Chin, M., Martin, R.V., 2003. Sources of carbonaceous aerosols over the united states and implications for natural visibility. Journal of Geophysical Research-Atmospheres 108, 4355.

Polidori, A., Turpin, B.J., Davidson, C.I., Rodenburg L.A., Maimone F., 2008. Organic PM 2.5 : Fractionation by Polarity, FTIR Spectroscopy, and OM/OC Ratio for the Pittsburgh Aerosol. Aerosol Science and Technology, 42:3, 233-246.

Pye, H.O.T., Liao, H., Wu, S., Mickley, L.J., Jacob, D.J., Henze, D.K., Seinfeld, J.H., 2009. Effect of changes in climate and emissions on future sulfate-nitrate-ammonium aerosol levels in the united states. Journal of Geophysical Research-Atmospheres 114, D01205.

Russell, L.M., Takahama, S., Liu, S., Hawkins, L.N., Covert, D.S., Quinn, P.K., Bates, T.S., 2009. Oxygenated fraction and mass of organic aerosol from direct emission and atmospheric processing measured on the R/V ronald brown during TEXAQS/GoMACCS 2006. Journal of Geophysical Research-Atmospheres 114, D00F05.

Setyan, A., Zhang, Q., Merkel, M., Knighton, W.B., Sun, Y., Song, C., Shilling, J.E., Onasch, T.B., Herndon, S.C., Worsnop, D.R., Fast, J.D., Zaveri, R.A., Berg, L.K., Wiedensohler, A., Flowers, B.A., Dubey, M.K., Subramanian, R., 2012. Characterization of submicron particles influenced by mixed biogenic and anthropogenic emissions using high-resolution aerosol mass spectrometry: Results from CARES. Atmospheric Chemistry and Physics 12, 8131-8156.

Simon, H., Bhave, P.V., Swall, J.L., Frank, N.H., Malm, W.C., 2011. Determining the spatial and seasonal variability in OM/OC ratios across the US using multiple regression. Atmospheric Chemistry and Physics 11, 2933-2949.

Simon, H. and Bhave, P.V., 2012. Simulating the degree of oxidation in atmospheric organic particles. Environmental science & technology 46, 331-339.

Spracklen, D.V., Jimenez, J.L., Carslaw, K.S., Worsnop, D.R., Evans, M.J., Mann, G.W., Zhang, Q., Canagaratna, M.R., Allan, J., Coe, H., McFiggans, G., Rap, A., Forster, P., 2011. Aerosol mass spectrometer constraint on the global secondary organic aerosol budget. Atmospheric Chemistry and Physics 11, 12109-12136.

Sun, Y., Zhang, Q., Macdonald, A.M., Hayden, K., Li, S.M., Liggio, J., Liu, P.S.K., Anlauf, K.G., Leaitch, W.R., Steffen, A., Cubison, M., Worsnop, D.R., van Donkelaar, A., Martin, R.V., 2009. Size-resolved aerosol chemistry on whistler mountain, canada with a high-resolution aerosol mass spectrometer during INTEX-B. Atmospheric Chemistry and Physics 9, 3095-3111.

Sun, Y., Zhang, Q., Zheng, M., Ding, X., Edgerton, E.S., Wang, X., 2011. Characterization and source apportionment of water-soluble organic matter in atmospheric fine particles (PM2.5) with high-resolution aerosol mass spectrometry and GC-MS. Environmental science & technology 45, 4854-4861.

Thornton, J.A., Jaegle, L., McNeill, V.F., 2008. Assessing known pathways for HO2 loss in aqueous atmospheric aerosols: Regional and global impacts on tropospheric oxidants. Journal of Geophysical Research-Atmospheres 113, D05303.

Turpin, B.J. and Lim, H.J., 2001. Species contributions to PM2.5 mass concentrations: Revisiting common assumptions for estimating organic mass. Aerosol Science and Technology 35, 602-610.

van Donkelaar, A., Martin, R.V., Leaitch, W.R., Macdonald, A.M., Walker, T.W., Streets, D.G., Zhang, Q., Dunlea, E.J., Jimenez, J.L., Dibb, J.E., Huey, L.G., Weber, R., Andreae, M.O., 2008. Analysis of aircraft and satellite measurements from the intercontinental chemical transport experiment (INTEX-B) to quantify long-range transport of east asian sulfur to canada. Atmospheric Chemistry and Physics 8,

Walker, J.M., Philip, S., Martin, R.V., Seinfeld, J.H., 2012. Simulation of nitrate, sulfate, and ammonium aerosols over the united states. Atmospheric Chemistry and Physics 12, 11213-11227.

Wang, Y.H., Jacob, D.J., Logan, J.A., 1998. Global simulation of tropospheric O-3-NOx-hydrocarbon chemistry 1. model formulation. Journal of Geophysical Research-Atmospheres 103, 10713-10725.

White, W.H. and Roberts, P.T., 1977. Nature and origins of visibility-reducing aerosols in los-angeles air basin. Atmospheric Environment 11, 803-812.

Yienger, J.J. and Levy, H., 1995. Empirical-model of global soil-biogenic nox emissions. Journal of Geophysical Research-Atmospheres 100, 11447-11464.

Xing, L., Fu, T.-M., Cao, J. J., Lee, S. C., Wang, G. H., Ho, K. F., Cheng, M.-C., You, C.-F., and Wang, T. J., 2013. Seasonal and spatial variability of the OM/OC mass ratios and high regional correlation between oxalic acid and zinc in Chinese urban organic aerosols. Atmospheric Chemistry and Physics 13, 4307-4318.

Zhang, Q., Streets, D.G., Carmichael, G.R., He, K.B., Huo, H., Kannari, A., Klimont, Z., Park, I.S., Reddy, S., Fu, J.S., Chen, D., Duan, L., Lei, Y., Wang, L.T., Yao, Z.L., 2009. Asian emissions in 2006 for the NASA INTEX-B mission. Atmospheric Chemistry and Physics 9, 5131-5153.

Zhang, Q., Jimenez, J.L., Canagaratna, M.R., Allan, J.D., Coe, H., Ulbrich, I., Alfarra, M.R., Takami, A., Middlebrook, A.M., Sun, Y.L., Dzepina, K., Dunlea, E., Docherty, K., DeCarlo, P.F., Salcedo, D., Onasch, T., Jayne, J.T., Miyoshi, T., Shimono, A., Hatakeyama, S., Takegawa, N., Kondo, Y., Schneider, J., Drewnick, F., Borrmann, S., Weimer, S., Demerjian, K., Williams, P., Bower, K., Bahreini, R., Cottrell, L., Griffin, R.J., Rautiainen, J., Sun, J.Y., Zhang, Y.M., Worsnop, D.R., 2007. Ubiquity and dominance of oxygenated species in organic aerosols in anthropogenically-influenced northern hemisphere midlatitudes. Geophysical Research Letters 34, L13801.

Zhang, Q., Alfarra, M.R., Worsnop, D.R., Allan, J.D., Coe, H., Canagaratna, M.R., Jimenez, J.L., 2005a. Deconvolution and quantification of hydrocarbon-like and oxygenated organic aerosols based on aerosol mass spectrometry. Environmental science & technology 39, 4938-4952.

Zhang, Q., Worsnop, D.R., Canagaratna, M.R., Jimenez, J.L., 2005b. Hydrocarbon-like and oxygenated organic aerosols in pittsburgh: Insights into sources and processes of organic aerosols. Atmospheric Chemistry and Physics 5, 3289-3311.

Zhang, Q., Jimenez, J.L., Canagaratna, M.R., Ulbrich, I.M., Ng, N.L., Worsnop, D.R., Sun, Y., 2011. Understanding atmospheric organic aerosols via factor analysis of aerosol mass spectrometry: A review. Analytical and Bioanalytical Chemistry 401, 3045-3067.

Figure Captions

Figure 1: Scatter plot of Aerosol Mass Spectrometer (AMS) measured OM/OC ratio, and the corresponding estimated primary organic aerosol fraction (f_{POA}) from several field campaigns around the globe. The dots and the corresponding numbers on the plot represent AMS field campaign mean values for (1) Whistler, Canada (Sun et al., 2009); (2) Long Island (Zhou et al., in preparation); (3) CARES T1 (Setyan et al., 2012); (4) Pearl River Delta, China (Huang et al., 2011); (5) SOAR 1 (Docherty et al., 2011); (6) New York City (Sun et al., 2011); (7) CalNex, Los Angeles (Hayes et al., 2013); (8) Beijing, China (Huang et al., 2010); (9) Fresno, California (Ge et al., 2012); and (10) typical urban POA (Jimenez et al., 2009). The solid black line is equation 1 (also in inset).

Figure 2: Aerosol Mass Spectrometer measured organic aerosol (OA), estimated primary OA (POA), POA fraction (f_{POA}), and predicted organic mass (OM) to organic carbon (OC) ratio using equation 1 (data source: Spracklen et al. 2011 and Zhang et al. 2007).

Figure 3: Scatter plot of estimated primary organic aerosol fraction (f_{POA}) from the Aerosol Mass Spectrometer (AMS) versus ground-level NO_2 concentrations derived from the OMI satellite instrument. The circled dots and the corresponding numbers represent outliers. The dots/numbers from 1 to 3 represent mean values for the New York City, Summer 2001; New York City, Winter 2004; and Vancouver, Canada, August 2001 campaigns respectively. The solid black line is equation 2 (also in inset).

Figure 4: Seasonal OM/OC ratio estimated from the prediction model (equation 3) using the OMI-derived ground-level NO_2 concentration. Seasons are defined as December-January-

633 February (DJF), March-April-May (MAM), June-July-August (JJA), and September-October-
634 November (SON).
635
636
637
638
639
640
641
642
643
644
645
646
647
648
649

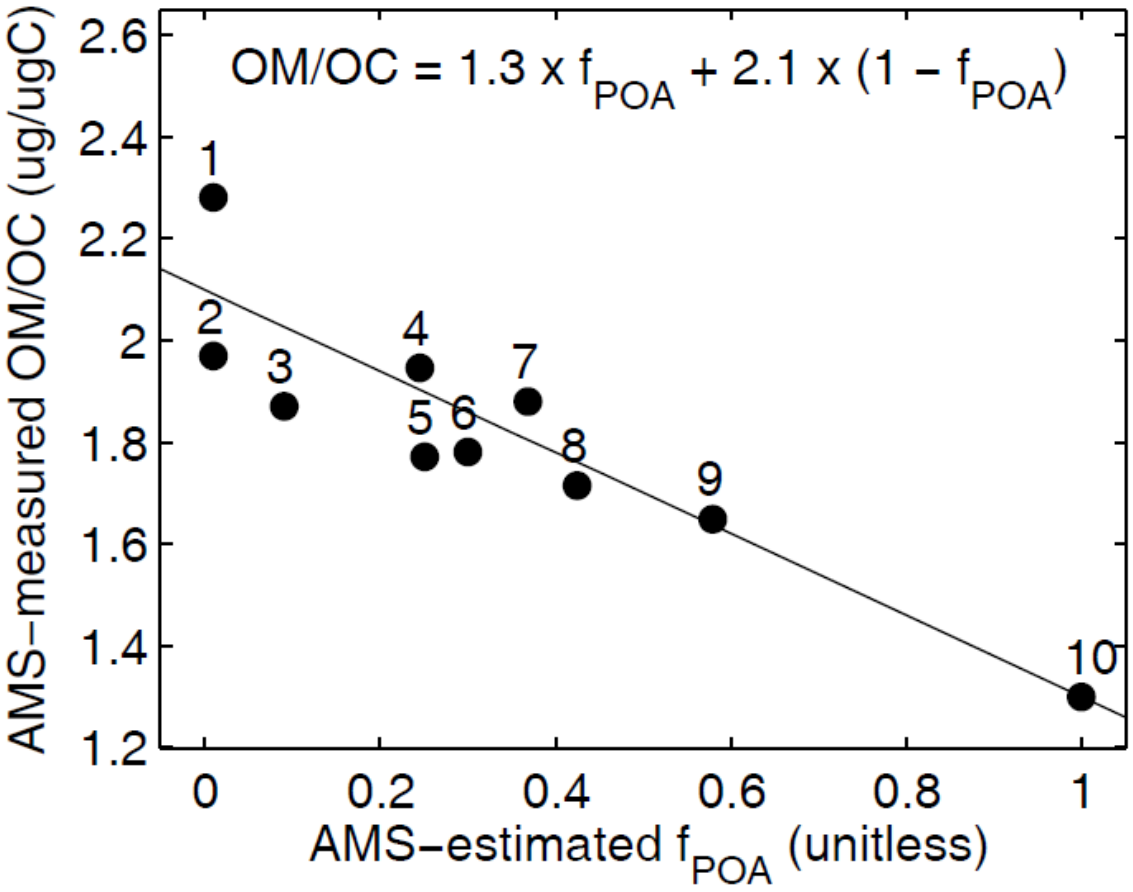

650

651 Figure 1.

652

653

654

655

656

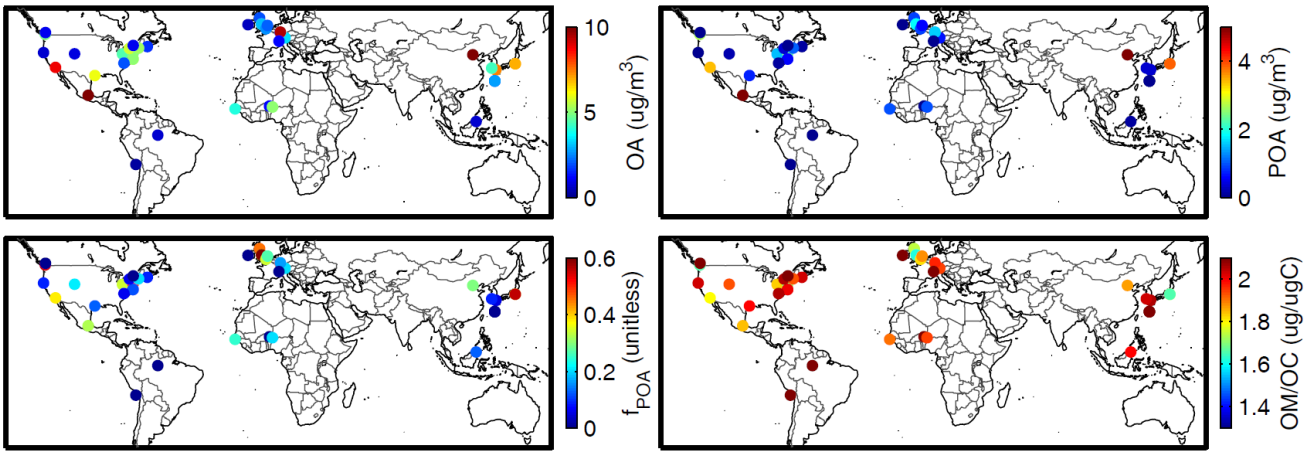
10
5
0
OA (ug/m3)
4
2
0
POA (ug/m3)
0.6
0.4
0.2
0
fPOA (unitless)
2
1.8
1.6
1.4
OM/OC (ug/ugC)

Figure 2.

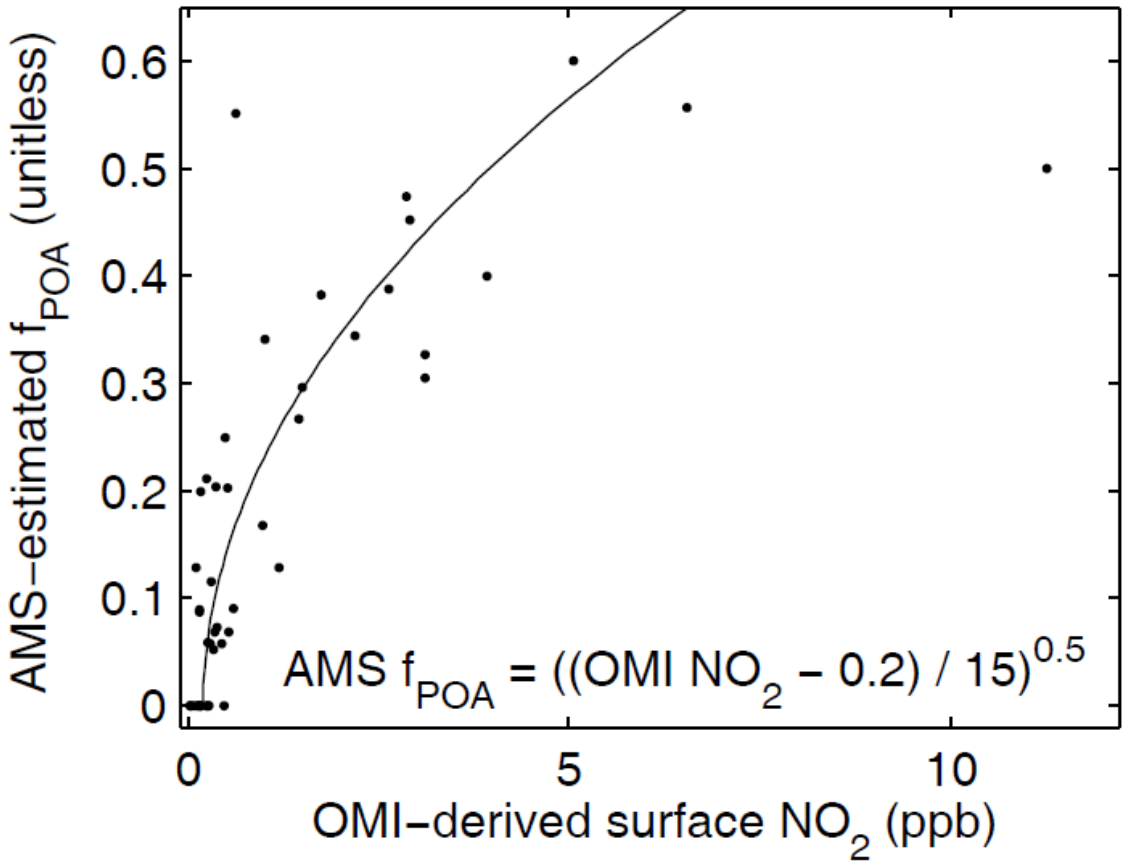

669

670 Figure 3.

671

672

673

674

675

676

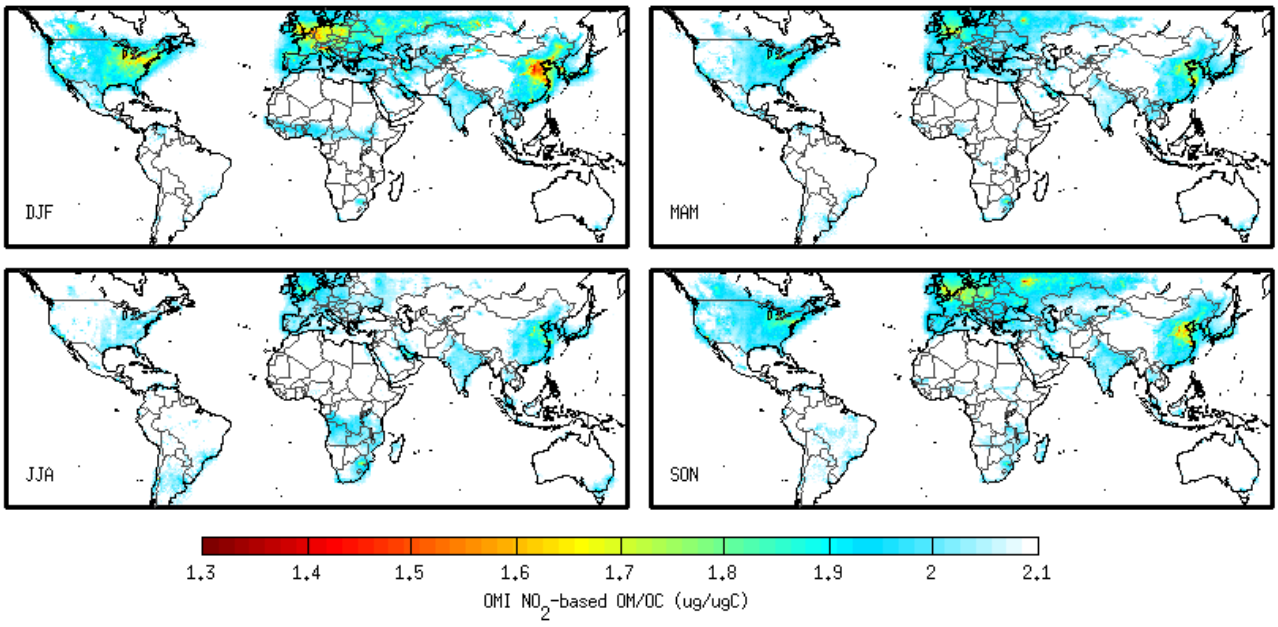

677

678 Figure 4.

679

680